JGR Biogeosciences

RESEARCH ARTICLE
10.1029/2022JG006922

Quantifying the Global Power Needed for Sap Ascent in Plants

Gregory R. Quetin[1], Leander D. L. Anderegg[2], Alexandra G. Konings[3], and Anna T. Trugman[1]

[1]Department of Geography, University of California, Santa Barbara, CA, USA, [2]Department of Ecology, Evolution, and Marine Biology, University of California, Santa Barbara, CA, USA, [3]Department of Earth System Science, Stanford University, Stanford, CA, USA

Key Points:

- Life on Earth is partially fueled by energy passively harvested from the environment to lift sap against frictional forces and gravity
- For the first time, we quantify sap ascent power globally with remotely sensed and field measurements of plant fluxes, states, and traits
- Sap ascent power is 14.2% the size of photosynthetic energy and comparable to the production of all hydropower across the globe

Supporting Information:

Supporting Information may be found in the online version of this article.

Correspondence to:

G. R. Quetin,
gquetin@ucsb.edu

Citation:

Quetin, G. R., Anderegg, L. D. L., Konings, A. G., & Trugman, A. T. (2022). Quantifying the global power needed for sap ascent in plants. *Journal of Geophysical Research: Biogeosciences*, *127*, e2022JG006922. https://doi.org/10.1029/2022JG006922

Received 8 APR 2022
Accepted 1 AUG 2022

Author Contributions:

Conceptualization: Gregory R. Quetin, Leander D. L. Anderegg, Anna T. Trugman
Funding acquisition: Alexandra G. Konings, Anna T. Trugman
Investigation: Gregory R. Quetin, Leander D. L. Anderegg, Anna T. Trugman
Methodology: Gregory R. Quetin, Leander D. L. Anderegg, Alexandra G. Konings, Anna T. Trugman
Supervision: Anna T. Trugman
Visualization: Gregory R. Quetin, Leander D. L. Anderegg, Anna T. Trugman
Writing – original draft: Gregory R. Quetin, Leander D. L. Anderegg, Anna T. Trugman

Abstract Terrestrial photosynthesis requires the evaporation of water (transpiration) in exchange for CO_2 needed to form sugars. The water for transpiration is drawn up through plant roots, stem, and branches via a water potential gradient. However, this flow of water—or sap ascent—requires energy to lift the water to the canopy and to overcome the resistance of the plant's water transporting xylem. Here, we use a combination of field measurements of plant physiology (hydraulic conductivity) and state-of-the-science global estimates of transpiration to calculate how much energy is passively harvested by plants to power the sap ascent pump across the world's terrestrial vegetation. Globally, we find that 0.06 W/m^2 is consumed in sap ascent over forest dominated ecosystems or 9.4 PWh/yr (equal to global hydropower energy production). Though small in comparison to other components of the Earth's surface energy budget, sap ascent work in forests represents 14.2% of the energy compared to the energy consumed to create sugars through photosynthesis, with values up to 18% in temperate rainforests. The power needed for sap ascent generally increases with photosynthesis, but is moderated by both climate and plant physiology, as the most work is consumed in regions with large transpiration fluxes (such as the moist tropics) and in areas where vegetation has low conductivity (such as temperate rainforests dominated by conifer trees). Here, we present a bottom-up analysis of sap ascent work that demonstrates its significant role in plant function across the globe.

Plain Language Summary Trees transpire up to 100 gallons of water per day, which requires energy to overcome gravity and the resistance of specialized stem transportation tissues. We show that the energy used by trees to move water from the soil to the leaves for transpiration is of the same order of magnitude to the energy harvested by these plants from sunlight during photosynthesis. This work implies that the evolution of vascular plants has created a pump that passively harvests energy to lift water to plant canopies, which is a significant energetic benefit to plant function and helps fuel life on Earth.

1. Introduction

Photosynthesis fuels life on Earth. The roots and stems of vascular plants made expansion of photosynthesis on land possible by mining water from the soils to supply water to the canopy where photosynthesis requires aqueous CO_2 (Berry et al., 2010). However, plant water is continuously lost to the dry atmosphere through evaporation (i.e., transpiration). This demand for water in the canopy presents a challenge for terrestrial plants, as transporting the water from soil to canopy requires energy to move water through the resistive conduits of the plant vascular system. Although the flow of energy to transport water through the plant is at the nexus of global photosynthesis, transpiration, and life on Earth, it has never been quantified.

The physical transport of water from the soil to plant canopies takes place primarily through plant xylem, specialized water-conducting tissue made up largely of xylem conduits constructed of dead cell walls. According to cohesion-tension theory (Dixon & Joly, 1895), water moves through these specialized xylem conduits under "negative pressure", pulled up to the leaf evaporative site by the tension of countless tiny menisci at the evaporative surface, capillary forces, and hydrogen bonds (Venturas et al., 2017). The structure of plants—canopy, stems, and roots—form a natural pump that helps create and harness the water potential gradient between the soil, canopy, and atmosphere, to move massive amounts of water. This "sap ascent" pump has to provide the energy required to lift water to the canopy against gravity as well as the energy to overcome the resistance produced by the plant's roots, stems, branches, and leaves to meet plant transpiration demands.

Writing – review & editing: Gregory R. Quetin, Leander D. L. Anderegg, Alexandra G. Konings, Anna T. Trugman

The energy to power sap ascent is drawn from the water potential gradient from the soil to the plant canopy, which is due to the evaporation of water molecules from transpiring leaves. Ultimately, this evaporation is possible because of the positive energy flux into the canopy. This positive energy flux is generally caused by solar radiation, and to a smaller extent longwave radiation and downward sensible heating. Plant hydraulic structures serve to passively transport water without requiring additional metabolic energy on the part of the plants, though metabolic energy is required to operate stomates and to build and maintain the plant's hydraulic structures (Schenk et al., 2020). The passive process of water movement through dead xylem cells transfers almost 40% of rainfall incident on land up to plant leaves to be transpired back to the atmosphere (Schlesinger & Jasechko, 2014). Indeed, plant transpiration is one of the most important components determining the land surface energy balance, land surface temperatures, and biosphere-atmosphere mass transfers (Bonan, 2008). Further, water movement through plants is central to plant physiology (Brodribb, 2009; Dixon & Joly, 1895), ecosystem function (Anderegg, Konings, et al., 2018), and global land-atmosphere interactions (Anderegg et al., 2019; Khanna et al., 2017).

Millions of years of evolution have worked to shape the effectiveness of the plant's "sap ascent pump." The fundamental need to provide water to the canopy to support transpiration has driven much of plant evolution and resulted in some of the world's most stunning biological structures. For instance, giant redwood trees, *Sequoiadendron gigantum*, can grow over 100 m tall and lift over 2,000 L of water per day to their canopies to support transpiration (Ambrose, 2016). But just how successful has this evolution been? Is the energy needed to power the movement of water from the soil to the canopy a large part of the energy supporting the biosphere or is it inconsequential? A combination of recent advancements in plant hydraulic measurements and global remote sensing allows us to answer for the first time: (a) how much energy does it take to power sap ascent and how does it vary across the globe? (b) Can variations in plants' hydraulic architectures drive variations in the energetic benefit of sap ascent or are variations driven primarily by climate? (c) How does the size of the sap ascent pump vary compared to metabolic energy available to plants through photosynthesis? (d) Are some ecosystems gaining proportionally more energy from their sap ascent pump in comparison to their metabolic processes?

2. Theory of Sap Ascent Power

The power required to move water through the body of a plant is analogous to water flowing through a pipe. To transport water through a pipe, a pump is needed to add pressure to the system to overcome the resistance (e.g., friction) inherent in the pipe. Energy is consumed by the pump to create this added pressure and maintain the flow of water (Figure 1a). Similarly, the movement of water during sap ascent in plants consumes energy over time, the "sap ascent power", to overcome the resistance of the body of the plant.

The "sap ascent work", can be calculated by considering the relationship between the resistance of the xylem, the volumetric flow, and the negative pressure between soil and canopy (the negative pressure created by the water lost in the canopy through transpiration; Figure 1b). Darcy's law, which governs the movement of water through a porous material, can be used to calculate the volumetric flow (Q) as the pressure change ($\Delta\Psi$) over the total plant resistance (R_{plant})—or rearranged, the pressure change is equal to the volumetric flow times the plant resistance (Equation 1; Reid et al., 2005):

$$\Delta\Psi = Q \times R_{\text{plant}} \tag{1}$$

Next, as a consequence of the conservation of energy in the Bernoulli equation, the power (P) maintaining the fluid flow across the pressure is equal to the volumetric flow times the drop in pressure (Equation 2):

$$P = Q \times \Delta\Psi \tag{2}$$

Making substitutions between Equations 1 and 2, the power required for sap ascent (P_{SA}) is equal to the volumetric flow of water squared, multiplied by the resistance of the plant plus the power to lift water against gravity to the canopy (see Material and Methods, Equation 8).

$$P_{\text{SA}} = Q^2 \times R_{\text{plant}} + P_{\text{gravity}} \tag{3}$$

Through conservation of mass, we substitute plant transpiration (T) for the volumetric flow. Here T is the mass flow of water (kg s^{-1}), which is more commonly observed and modeled, such that $Q = \frac{T}{\rho_w}$, where ρ_w is the density of water (Equation 3; Granier, 1987):

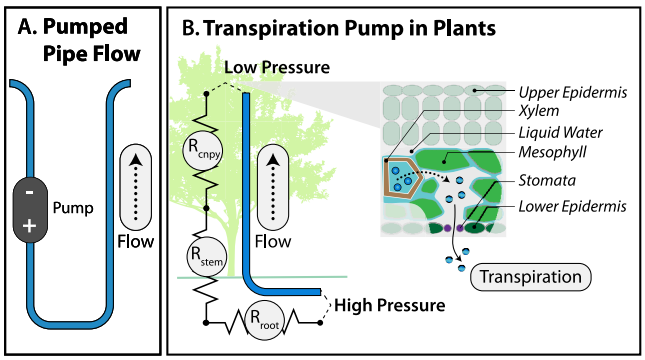

Figure 1. Transpiration drives a pump that overcomes resistance in plants to power sap ascent, moving water from the soil to the canopy. To move water in a pipe, a pump must expend energy to overcome the resistance of the pipe by increasing the pressure (A). In plants, transpiration serves to power a pump needed to overcome the resistance of the plant hydraulic pathways (R_{root}, R_{stem}, and R_{cnpy}) during sap ascent through roots, stem, and canopy (B). Inset (B) shows diagram of plant leaf, including xylem, photosynthetic mesophyll cells, and the evaporation of water molecules (blue circles) into the leaf intercellular airspace that creates negative pressure in the xylem.

$$P_{SA} = \left(\frac{T}{\rho_w}\right)^2 \times R_{plant} + P_{gravity} \quad (4)$$

The total plant resistance (R_{plant}) includes the resistance of the plant roots, stem, and canopy. Although the resistance of stomates is critical in controlling the rate of transpiration, once the water evaporates in the intercellular air space in the leaf mesophyll, most of the water vapor does not require any energy to diffusively pass through the stomatal pore according to Fick's Law of Diffusion (Figure 1b). At very high temperatures it is possible for a small portion of the water vapor in transpiration to pass out of the stomata nondiffusively (Kowalski, 2017). However, this "stomatal jet" does not consume significant power as the stomatal resistance is many orders of magnitude smaller than the plant hydraulic resistance. Thus, P_{SA} does not directly depend on stomatal closure except insofar as that stomatal closure is reflected in T.

The resistance of the xylem and other plant organs is the inverse of the more commonly reported plant conductance (k_{plant}, kg MPa^{-1}s^{-1}) and can be estimated from field-based measurements of the conductance per leaf (k_L, kg m^{-2} MPa^{-1}s^{-1}) and conductivity per unit leaf area (K_L, kg m^{-1} MPa^{-1}s^{-1}) where k_L is normalized by leaf area and K_L is normalized by leaf area over branch length. Whole plant conductance is estimated differently for woody and nonwoody plants due to difference in their standard measurement techniques (see Materials and Methods).

For our global analysis, we calculated the sap ascent power per area of grid cell (p_{SA}) using measured transpiration per area (J) and the resistance of plants for an area (r_{plant}; Equation 5):

$$p_{SA} = \left(\frac{J}{\rho_w}\right)^2 \times r_{plant} + p_{gravity} \quad (5)$$

For woody plants, conductance is typically measured per branch, and can be scaled to a plant-scale value based on information on canopy height, leaf area, and the allometric ratio of stem resistance to whole plant resistance. For nonwoody plants, the conductance is typically measured per leaf and can be scaled based on leaf area and the allometric ratio of leaf resistance to whole plant resistance. For the global analysis, the plant conductance is scaled by leaf area index ($a_{LAI} = \frac{A_{leaf}}{A_{ground}}$) to provide plant conductance per area that is inverted to r_{plant}. See Supporting Information S1 for method of land cover type weighting and a detailed unit analysis. For an individual plant, Equations 1–4, allows the power required for sap ascent to be calculated from transpiration, height, leaf area, conductivity, and common allometric relationships, while Equation 5 extends this to calculating the power density required for sap ascent using observations of the transpiration water flux per area and the leaf area index. Table 1 summarizes the input data sources and data sets, and Table S1 in Supporting Information S1 summarizes units of other values (see Materials and Methods).

3. Materials and Methods

We calculated the amount of power involved in three critical plant physiological functions for cross-comparison: moving water from the soil to the evaporative sites in leaves (i.e., sap ascent power), vaporization of water during transpiring (latent heat), and fixing CO_2 through photosynthesis (power of gross primary production). To calculate sap ascent power we developed a global map of whole plant resistance. Additionally, we compared our global estimate of sap ascent power using biome average hydraulic traits with our analysis for the contiguous United States, where spatial variation in ecosystem average or "community-weighted mean" hydraulic traits have been quantified for U.S. forests based on high resolution forest inventory data of species' distributions and abundances (Trugman et al., 2020).

Table 1
Data Sources and Variables Used in the Calculation of Sap Ascent Power

Variable	Name	Units	Data Set
J	Transpiration water flux per area	kg m^{-2} s^{-1}	Multiple[a,b]
ρ_w	Density of water	kg m^{-3}	1,000
K_L	Conductivity per unit leaf area	kg m^{-1} MPa^{-1} s^{-1}	XFT[c]
k_L	Conductance per leaf	kg m^{-2} MPa^{-1} s^{-1}	XFT[c]
h	Tree height	m	Lidar (Simard et al., 2011)
a_{LAI}	Leaf area index	m^2/m^2	LAI3g (Zhu et al., 2013)
f_{woody}	Allometric stem fraction	N/A	0.25 (Sack et al., 2003; Sack & Tyree, 2005; Sperry et al., 2017)
f_{nonwoody}	Allometric leaf fraction	N/A	0.25 (Sack et al., 2003; Sack & Tyree, 2005; Sperry et al., 2017)

[a]Global Land Evaporation Amsterdam Model (GLEAM) v3.3b data set (Martens et al., 2017). [b]Global Land Data Assimilation System (GLDAS-2.1) data set (Hiroko et al., 2016). [c]Xylem Functional Trait database (Gleason et al., 2016).

3.1. Scaling Conductivity to the Globe

To map plant resistance across the globe we first grouped species-level conductivity (conductance per conductor length) per unit leaf area (K_L) measurements by biome to calculate the median biome-level K_L plus within-biome interquartile range and full range in K_L. For nonwoody plants, we did the same with conductance per unit leaf area (k_L) an alternate normalization for nonwoody plants. We determined the conductance of each biome type by multiplying the normalized plant level values of K_L or k_L (each normalized by length and leaf area, or just leaf area) by LAI (leaf area per area of ground) and dividing by plant height (length) for forests and multiplying by LAI alone for grasses, forbs, and crops (Figures S1–S6 in Supporting Information S1). We then weighted each biome conductance according to fractional land cover type (combining grasses, forbs, and crops into a single "non-forest" cover type) to get ecosystem-scale average hydraulic conductance before inverting to recover resistance for each grid cell.

3.2. Assigning K_L Values to Different Biome Types

To estimate K_L values across the globe, each entry in the Xylem Functional Trait (XFT) database reporting K_L or for which K_L could be calculated from stem specific conductivity (K_S) and leaf:sapwood area (A_L:A_S; 703 measurements from 534 species, including 324 genera and 108 families) was assigned to an IGBP land cover type (Gleason et al., 2016). In the XFT data set, we could not distinguish "Open Shrubland", "Closed Shrubland", and "Savanna" (woody or otherwise) plants. Instead, we combined all nonforest shrubs and lumped them into "Combined Shrubland." We maintain the biome designations of "Open Shrubland" and "Closed Shrubland" only to show fractional land cover (Figure S3 in Supporting Information S1). In addition, we do not attempt to ascribe a value to "Savanna" biome-types in our analysis, instead leaving points dominated by "Savanna" biome-type blank. Trees were assigned to IGBP land cover categories based on whether they were gymnosperm or angiosperm and evergreen or deciduous. In general, there is a very large variation of K_L within groups, cover types, and biomes, with little of the within-group variation easily explained with climatic factors for the majority of cover types. The resulting K_L values by land cover category appear relatively log normal, and the K_L uncertainty was calculated for each land cover as the min, max, median, and interquartile range.

Branch K_L was then scaled to whole plant K_L for a biome by assuming that ~25% of plant resistance is in the stem for woody plants (Sack & Tyree, 2005; Sperry & Love, 2015), that is, by assuming a stem factor f_{woody}. Conversion to full plant resistance in forests is then calculated as (Equation 6):

$$r_{\text{plant}} = r_{\text{woody}} = \frac{r_{\text{stem}}}{f_{\text{woody}}} = \left(\rho_w \times \frac{1}{K_L} \times \frac{h}{a_{\text{LAI}}}\right) \frac{1}{f_{\text{woody}}}, \quad (6)$$

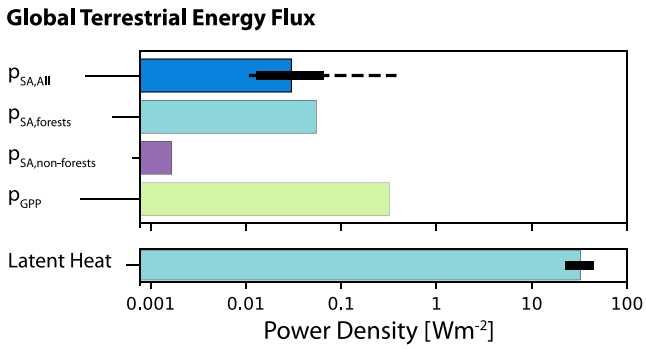

Figure 2. Global estimates of the average sap ascent power density (p_{SA}) compared to the energy captured during photosynthesis and the latent heat flux from the land surface. The power density used to lift water against gravity and overcome the hydraulic resistance of xylem vessels can be compared to the density of power used to fix sugars in photosynthesis (p_{GPP}), and to the density of power needed to vaporize water in transpiration (i.e., latent heat). Estimates of these energy fluxes for global values ($p_{SA,All}$), and over forests ($p_{SA,forests}$), and nonforests ($p_{SA,nonforests}$) are shown. Solid line in $p_{SA,All}$ shows the interquartile range based on conductivity, while the dashed line shows the minimum to maximum range based on conductivity. Dark line in latent heat is the range due to uncertainty across transpiration data products (see Table 1).

where resistance (r_x) was scaled to the whole plant and per area by height (h) and leaf area index (a_{LAI}; see Table 1, Table S1 in Supporting Information S1, and Supporting Information for units).

For nonwoody plants (grass, forb, and crops), leaf area-specific conductance k_L, species average values were collated from the literature (see *Data* below). Each average was weighted by the number of species for entries where the reported K_L value was already the average of multiple species. Grasslands are the average value of all noncrop grasses (36 species for which K_L data was available), and crops are the average of grass and herb crops (27 species or cultivars) for the Grasslands and Crops IGBP category. Note that there was not sufficient data to distinguish between C4 and C3 grasses. Leaf area-specific conductance was then scaled to whole plant conductance by assuming ~25% of whole plant resistance is in the leaves for nonwoody plants (Sack & Tyree, 2005), using the factor $f_{nonwoody}$. Unlike for woody plants, this scaling does not need to be multiplied by path length (i.e., height) because the leaf-scale measurements of k_L for these types of species are not determined by path length. Conversion to full plant resistance in nonwoody plants (Equation 7):

$$r_{plant} = r_{nonwoody} = \frac{r_{leaf}}{f_{nonwoody}} = \left(\rho_w \times \frac{1}{k_L} \times \frac{1}{a_{LAI}}\right) \frac{1}{f_{nonwoody}} \quad (7)$$

3.3. Mapping Conductivity Globally

The conductivity values estimated for each biome were extended to the globe using the moderate resolution imaging spectroradiometer (MODIS) IGBP biome data set (Sulla-Menashe et al., 2019). Before calculating the ecosystem resistance and sap ascent power, the IGBP data set was regridded to 0.5° resolution to best match the *US forest Service Forest Inventory and Analysis Program* (FIA) data for comparison and for use of transpiration in the calculation. The grid point (or ecosystem scale) K_L values were calculated by first estimating the K_L values and their uncertainty for each biome from data (see above), and then multiplying the fraction of a particular biome in that grid point by the K_L of that biome. Each of these grid scale K_L values was then scaled to r_{plant} by the grid cell height, a_{LAI}, and allometry as appropriate per biome (i.e., woody or nonwoody). At these relatively coarse scales our analysis will not resolve the finer scale variations in K_L due to species or competitive environment (Brum et al., 2019).

The r_{plant} values were then summed at each grid point and normalized by the total fractional coverage of the biomes for which we had trait data (see Equations 4 and 8). We removed grid cells without at least 75% of the coverage from biomes with K_L in our data set. In addition, for analysis in Figures 2, 3, and 5, we determined whether a grid point was "forest dominated" or "nonforest dominated" by whether at least 75% of the land fraction was a forest biome or an herbaceous biome. Here 75% was chosen as a reasonable threshold where the conductivity of that ecosystem was well represented by the dominant vegetation coverage (Figure S6 in Supporting Information S1). This method of extending K_L values to the globe does not take into account separate species distributions and assumes that the a_{LAI} and transpiration are allocated to biomes by their fractional coverage of a grid point.

Our ground-up approach would benefit from future research measuring hydraulic traits across climate gradients for similar vegetation or across gradients for ecosystems with similar gross primary productivity (GPP). Additionally, estimations of sap ascent power can benefit from efforts to retrieve whole ecosystem hydraulic characteristics like conductivity from an inverse analysis (Liu et al., 2021).

3.4. Extending Sap Ascent Power to the Ecosystem Scale

The power needed to move water through vegetation can be estimated from commonly measured fluxes and characteristics of the ecosystem and allometric scaling (Equations 1–3). Where power overcoming plant resistance is calculated as the volumetric flow squared times the resistance of the plant. To extend this calculation to an

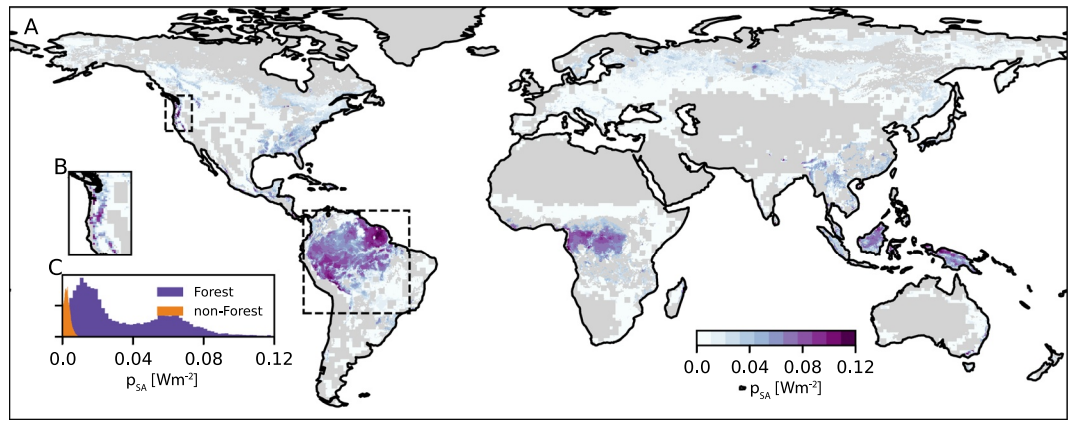

Figure 3. Global sap ascent power density p_{SA} for both forests and nonforests mapped globally (A). Expanded view (inset) of the sap ascent power density (for forests only) in the Pacific Northwest (B) and the frequency distribution across space for the globe (inset; C). Dashed frames denote the extent of the regions reported as the Pacific Northwest (B) and the Amazon.

ecosystem scale where transpiration per area (J) is measured for the ecosystem but conductivity is estimated by biome we estimated ecosystem conductance by an area weighted sum (Equation 8):

$$p_{\mathrm{SA}} = \left(\frac{J}{\rho_w}\right)^2 \times \frac{\rho_w}{A_{\mathrm{ground}} \times a_{\mathrm{LAI}}} \left(\frac{1}{h} \times f_{\mathrm{woody}} \times \sum\nolimits_n (K_{\mathrm{Ln}} \times A_n) + f_{\mathrm{nonwoody}} \times \sum\nolimits_m (k_{\mathrm{Lm}} \times A_m)\right)^{-1} + p_{gravity} \tag{8}$$

where ρ_w is the density of water, A is the grid cell area for each biome (m, n), a_{LAI} is the grid cell average a_{LAI}, h is the canopy height in meters, f_{woody} is the fraction of total plant resistance in stems for woody plants (=0.25, Sack et al., 2003; Sack & Tyree, 2005; Sperry et al., 2017), f_{nonwoody} is the fraction of total plant resistance in leaf tissues (=0.25, Sack et al., 2003; Sack & Tyree, 2005; Sperry et al., 2017), for woody biome type n and nonwoody biome type m. There is a small amount of additional power needed for sap ascent expended against gravity moving the water to the height of the canopy. We estimate the power per area needed to overcome the gravity potential in sap ascent based on the measured transpiration and height of the canopy (Equation 9):

$$p_{\mathrm{gravity}} = J \times g \times h \tag{9}$$

where g is the gravitational constant. The power needed to overcome the plant hydraulic resistance and the power to lift the water combine to make up the sap ascent power, integrated over time they are the sap ascent power needed to supply the canopy with water (Figure S7 in Supporting Information S1). The energy in sap ascent power is passively harvested by vegetation through transpiration in the canopy.

The average power for sap ascent was calculated for each month for the seasonal climatology of transpiration and a_{LAI}. These monthly values were then average to create annual values the power need for sap ascent or multiplied by time to calculate sap ascent work. Sap ascent power was set to zero for months where a_{LAI} was less than 0.1 to avoid dividing by small numbers when calculating the plant stem resistance during nonvegetated months in regions with high seasonality. In addition, sap ascent power and the power to overcome gravity potential were calculated with two independent transpiration data sets (see *Data*). The uncertainty due to transpiration was estimated, while the mean of the two estimates was generally used unless otherwise noted (i.e., Figures 3–6). Figures of the calculation with each transpiration data set separately are in the Supplement (Figures S13–S15 in Supporting Information S1).

3.5. Additional Uncertainty in Sap Ascent Power

There are three key assumptions that create additional uncertainty in our calculation of sap ascent power: (a) that the flow through the plant is equal to transpiration, (b) that the operational resistance is the minimum resistance, and (c) the allometric relationship between measured stem resistance and whole plant resistance is consistent

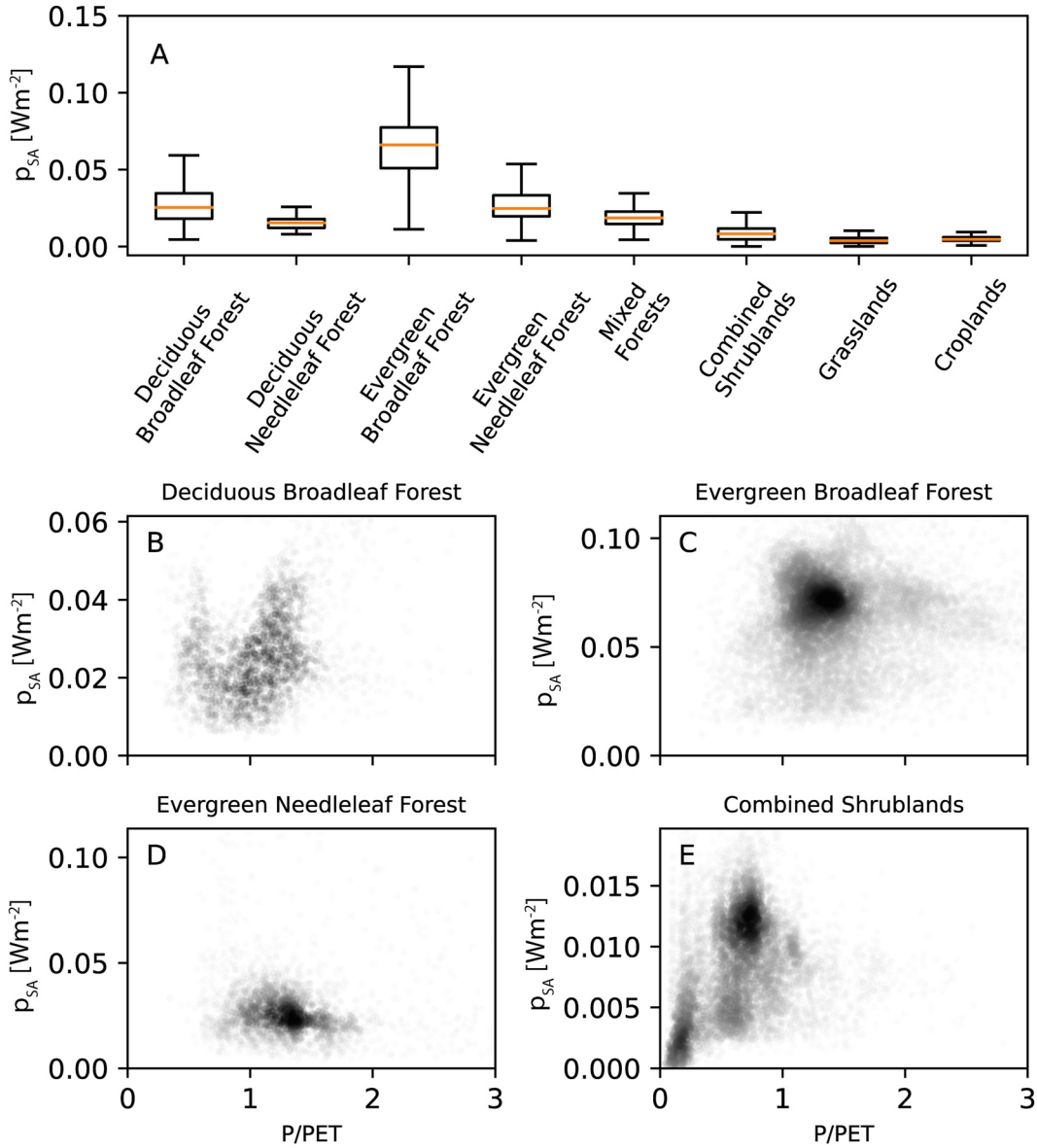

Figure 4. The variation of sap ascent power density (p_{SA}) across land cover type (A) and aridity (B–E). Aridity defined as precipitation over the potential evapotranspiration (P/PET). In (A), the orange line denotes median, box and whiskers show 25th–75th, the 5th–95th across space. In (B–E), shading represents the density of spatial points that occur with darker shading corresponding with a higher point density. Note, *y*-axis on subplots (B–E) differ per panel to highlight each pattern.

globally. First, in some regions, plants complicate the $Q = \frac{T}{\rho_w}$ assumption by absorbing water from the atmosphere. However, regions where this behavior is dominant are confined to small regions of cloud forest (0.26% of land area in the present; Bubb et al., 2004) and are only a small fraction of the total transpiration in other regions for specific species (e.g., Coastal California Redwoods; Burgess & Dawson, 2004). Second, due to high negative water potentials, it is possible that operational resistance would be higher than minimum resistance under some conditions. We do not expect variations in operational resistance to be a driving factor in sap ascent power as very little transpiration occurs once embolism starts. Additionally, even assuming a large 20% reduction in operational conductance across all transpiration, we would expect an increase in our sap ascent power estimate of only 25%. Third, the fraction of resistance allocated to the plant stems (assumed to be 25% in woody plants for our main analysis) remains poorly quantified (Sack & Holbrook, 2006), with one theoretical study estimating 80%–98% of resistance being allocated to leaves (Lechthaler et al., 2020). Using this extreme value, we would estimate that measurements of stem resistance was only 1.0%–20% of the total plant resistance—equivalent to a

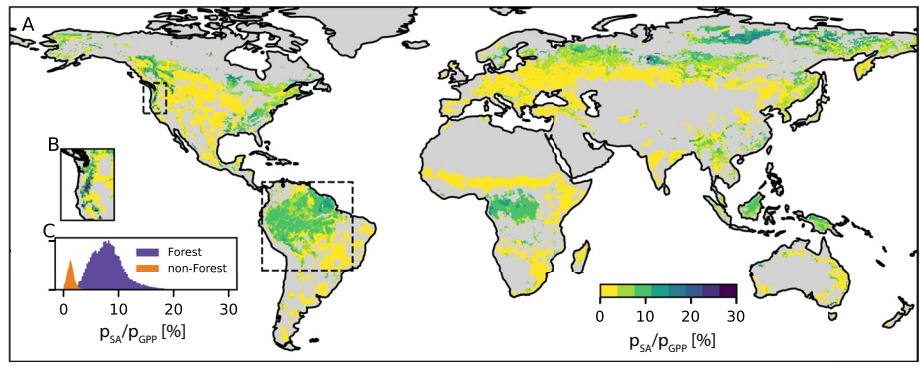

Figure 5. Ratio of the power density required from sap ascent (p_{SA}) to the power captured through photosynthesis (p_{GPP}). Mapped across the globe (A). Expanded view of the ratio of sap ascent power density to photosynthesis power density (inset, for forests only) in the Pacific Northwest (B) and as a distribution across the globe (inset; C). Dashed frames denote the extent of the regions discussed as the Pacific Northwest (B) and the Amazon.

$f_{woody} = 0.01 - 0.20$. Applied across all ecosystems this large estimate of the fraction of plant resistance in leaves would lead to a sap ascent power estimate 1.25–25 times larger than our current estimate. Though these assumptions contain significant uncertainty, they generally skew toward higher sap ascent power values and are all less than the uncertainty contained across the approximately 40× range from minimum to maximum of measured conductance per biome.

3.6. Power in Photosynthesis

For comparison to the energy harvested for sap ascent power, we calculated the energy flux of photosynthesis or photosynthetic power (P_{GPP}), which can be computed per mole as the energy in 18 adenosine triphosphate (ATP) molecules, which provide energy to drive most processes in living cells, divided by the energy in six CO_2 molecules. The "photosynthetic power" was calculated as the integration over time of the energy used in fixing a mole of CO_2 via ATP hydrolysis to ADP in the Calvin Cycle of photosynthesis multiplied by the rate of fixation (Equation 10):

$$p_{GPP} = \frac{GPP}{C \text{ molar mass}} \times \frac{18 \text{ ATP}}{6 \text{ CO2}}, \tag{10}$$

where GPP is the carbon flux per area of GPP, resulting in photosynthetic power density (p_{GPP}) and C molar mass is the molar mass of carbon. For each six CO_2 fixed by the Calvin Cycle, 18 ATP are used. We used 30 kJ/mol for ΔG of ATP (where G is Gibbs Free Energy is determined from the chemical structure), a value which is within the range of 28–34 kJ/mol measured for standard condition. Thus, ΔG of fixing 1 mol CO_2 is 90 kJ/mol (e.g., three times ΔG of ATP). For example, a globally integrated annual estimate for GPP of 147 Pg C from Badgley et al. (2019) and an estimated land surface area of 1.4894E8 km^2 results in the globally integrated power in photosynthesis of 0.23 W/m^2. Using a different estimate of globally integrated annual GPP of 123 Pg C (Beer et al., 2010), this number is reduced to 0.20 W/m^2.

We then created a spatially explicit map of the power in photosynthesis using the GPP map from Badgley et al. (2019) (used in Figures 5, 6, and Figure S8 in Supporting Information S1). Note that our method differs from the measurement of the energy stored in the bonds of a sugar molecule, which produces a GPP to energy estimate that is about a factor of four larger (Monteith, 1972).

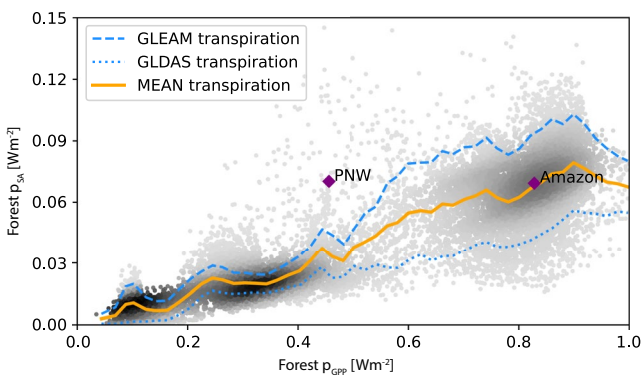

Figure 6. The power density needed for sap ascent (p_{SA}) relative to the power density needed to fix carbon in gross primary productivity (p_{GPP}) in forested regions. Dark shading represents a higher density of points. Purple diamonds represent reference regions in Fig. 5 including the Amazon in South America and the Pacific Northwest (PNW) in the continental US.

3.7. Data

3.7.1. XFT Database for K_L

The values of stem xylem conductivity per unit leaf area conductivity (K_L) normalized by path length for woody plants (kg m^{-1} MPa^{-1} s^{-1}) were aggregated from the XFT Database (Gleason et al., 2016). This database is a collection of measurements of plant hydraulics from around the globe (Figure S1 in Supporting Information S1), and we utilized all entries that either reported K_L directly or reported both K_s and A_L:A_S (n = 703 total measurements), primarily from stems. We excluded measurements that were not attributed to a biome, and measurements from seedlings, greenhouse rather than outdoor (natural, common garden, or outdoor experiment) studies, nonwoody tissues (petioles), cacti, and lianas. Additionally, we removed a small subset (23) of extremely high K_L outliers (K_L > 0.02 kg m^{-1} MPa^{-1} s^{-1}, or 100× the rest of the data set and far outside the observed log-normal distribution of K_L), which likely represented methodological or unit errors.

For nonwoody plants, species average leaf area-specific conductance data (k_L, mmol H_2O m^{-2} MPa^{-1} s^{-1}, or the conductance of the entire leaf organ, or often entire plant, per unit leaf area, which are then converted to kg m^{-2} MPa^{-1} s^{-1}) for nonwoody plants (grasses and forbs, both wild and crops) were collated from (Holloway-Phillips & Brodribb, 2011; Ocheltree et al., 2020, 2016; Pathare et al., 2020; Sack & Holbrook, 2006; Scoffoni et al., 2011; Xiong & Flexas, 2018). The XFT data can be accessed through TRY Plant Trait Database (Dataset 241: https://www.try-db.org/de/Datasets.php).

3.7.2. FIA Conductivity Data

We used a gridded data set of community weighted mean K_L values weighted by species' basal area abundance within a forest plot averaged to the grid cell level from Trugman et al. (2020). Data on species distribution and abundance were derived from the FIA long-term permanent plot network and species-level mean K_L values were derived from plant hydraulic traits database, the XFT database (Gleason et al., 2016). For this analysis, we gridded the plot-level FIA data from Trugman et al. (2020) at 0.5° resolution by computing a grid-level mean of plot-level community weighted mean K_L values within a given grid cell.

3.7.3. Transpiration

We used two transpiration data sets that are calculated through a combination of observations and models. We used the monthly climatology of transpiration for 2003–2018 from Global Land Evaporation Amsterdam Model (GLEAM) v3.3b data set (Martens et al., 2017). GLEAM is based on a combination of observations and modeling, combined using data assimilation. We also used the monthly climatology of transpiration for 2003–2018 from Global Land Data Assimilation System (GLDAS-2.1) Noah model outputs (Hiroko et al., 2016; Rodell et al., 2004). GLDAS-2.1 is a land surface model forced by observations.

3.7.4. Leaf Area Index

We used a monthly climatology from 1982 to 2011 of observationally based LAI estimates derived from a combination of optical observations from the MODIS and the advanced very high resolution radiometer (AVHRR; Zhu et al., 2013). The data was interpolated from 1.0° to 0.5° to match other data sets.

3.7.5. Height

We used a lidar-based tree size data set with a resolution of 1° latitude and longitude (Simard et al., 2011).

3.7.6. Gross Primary Productivity

We used an annual global estimate of GPP derived from MODIS near-infrared measurements (NIR_V) and a statistical relationship with flux towers (Badgley et al., 2019). The gridded data set was interpolated from 0.25° latitude-longitude to 0.5° latitude-longitude to match the resolution of other data sets.

3.7.7. Aridity, Precipitation Over Potential Evapotranspiration

We used precipitation from the Climate Research Unit (CRU) and reanalysis data from National Centers for Environmental Prediction (NCEP), the CRUNCEP data set (Viovy, 2018). In addition, we used monthly potential evapotranspiration from the GLDAS (Feng & Fu, 2013).

4. Sap Ascent Power and the Global Energy Cycle

To estimate sap ascent power across the globe, we combined maps of transpiration derived from a combination of models and observations (Hiroko et al., 2016; Martens et al., 2017) with a spatially explicit global map of plant resistance that we developed using a database of spatially distributed field-based measurements of K_L (Choat et al., 2012) extended globally through biome land cover fractions, global leaf area index (Zhu et al., 2013), and height (Simard et al., 2011; see Materials and Methods and Figure S1–S6 in Supporting Information S1).

The transpiration products that we used incorporate the response of stomata to environmental conditions (e.g., vapor pressure deficit, sunlight, and temperature) and soil moisture. Estimating evapotranspiration and separating it into transpiration, evaporation, and canopy interception is still uncertain (Stoy et al., 2019; Talsma et al., 2018). To estimate uncertainty due to this divergence in global transpiration estimates, we separately calculate sap ascent power from two established transpiration data sets (See Materials and Methods; Hiroko et al., 2016; Martens et al., 2017).

We assumed plants are working at their maximum potential conductivity (K_L in well hydrated tissues without any xylem embolism, known as K_{max}), as this value is both widely reported across studies and likely to represent plant conductivity at which most transpiration occurs (Brodribb et al., 2020; Choat et al., 2018; Delzon & Cochard, 2014; Sack & Scoffoni, 2012). In addition, the use of K_{max} yields the low-end (conservative) estimate of sap ascent power. Any decreased conductivity (increased resistance) from drought stress, freeze-thaw embolism, etc would increase whole plant resistance and thus increase estimates of sap ascent power. While the operational resistance of many plants may be more than minimum resistance (i.e., measured conductivity), it is uncommon for there to be large amounts of transpiration during periods of high plant resistance as the stomata respond to limit potentially damaging levels of water stress before it can increase xylem resistance (Anderegg, Wolf, et al., 2018; Delzon & Cochard, 2014; Sack & Scoffoni, 2012; Sperry et al., 2016). We used the range of reported values per biome (minimum, lower quartile, upper quartile, and maximum) to assess uncertainty in global sap ascent power due to conductivity.

We estimate that the global average power needed for sap ascent is 0.03 W/m^2 (interquartile range 0.02–0.04 W/m^2; Figure 2). The sap ascent power is much higher in regions dominated by forests (0.06 W/m^2, interquartile range 0.05–0.1 W/m^2) compared to regions of nonforested vegetation (0.003 W/m^2; Figure 2). In forests, power estimates are based on the median value of conductivity for each biome, which varies globally according to global biome maps, and includes the power needed to lift water to the canopy height ($p_{gravity}$, a small contribution at 0.005 W/m^2; Figure S7 in Supporting Information S1, Equations 9 and 10).

Though operating passively, sap ascent power supports the function of vascular plants by overcoming xylem resistance and gravity to supply water to the canopy to replace water lost through transpiration while stomates remain open to fuel photosynthesis. In conjunction, photosynthesis converts sunlight to sugars that power the metabolism of plants, and through them much of the Earth;s biosphere. To compare with sap ascent power density, the energy flux per area collected through photosynthesis (p_{GPP}) can be calculated per mole and integrated to the globe (see Materials and Methods).

Sap ascent power provides a substantial amount of passive energy collected by the plant. Indeed, in regions dominated by forests sap ascent power provides an additional 14.2% (p_{SA}/p_{GPP} based on median biome resistance) to the energy captured by photosynthesis. This estimate ranges from 11.3% to 23.1% based on the 25th–75th percentiles of biome resistance, while the estimate based on maximum biome resistance is >200% of photosynthetic power (Figure 2). In contrast, sap ascent power is a much smaller percentage of photosynthetic power in nonforest ecosystems at 1.3%.

The ultimate source of the power required for sap ascent is provided through evaporation of water into the intercellular airspace within the leaf as part of transpiration. This evaporation establishes the negative water potential between the soil and the canopy. While environmental conditions governing the rate of transpiration are complex—including the behavior of stomata, soil water conditions, and atmospheric dryness—there is a certain amount of energy required to overcome latent heat and vaporize water before it passes to the atmosphere through the stomata. The energy flux required to vaporize water during transpiration (~30 W/m^2 globally) is much larger than the energy flux for sap ascent (0.03 W/m^2 globally) but both are drawn from the same source (see Methods and Materials, Figure S9 in Supporting Information S1). The energy required for evaporation—and

thus for sap ascent—is primarily provided by downward shortwave radiation from the sun (~160 W/m^2 at the surface globally), and, to a much lesser extent, energy from downwelling longwave radiation and sensible heat into the canopy (Figure 1 and Figure S9 in Supporting Information S1). These energy sources are separate from the metabolism of the plants powered by photosynthesis.

Even though sap ascent power is small in comparison with the energy fluxes of the surface energy budget, when ranked alongside the scale of human endeavors, the total sap ascent work done by terrestrial ecosystems is large, especially in forests. The global annual sap ascent work done by forests is 9.4 PWh/yr (interquartile range 7.4–15.4 PWh/yr based on per biome conductivity, see Materials and Methods). The median estimate nears the total production of all hydropower across the globe (10.5 PWh in 2019), while the upper bound (e.g., minimum biome K_L) estimate of annual sap ascent work (~140 PWh/yr) would approach the total annual power production of humanity (173 PWh in 2019; Ritchie, 2019). In short, through millions of years of evolution, plants have passively harnessed an amount of energy to pump water to their canopies and fuel life on Earth equivalent to the industrial energy of humans.

5. Sources of Uncertainty in Quantifying Sap Ascent Power

Our results indicate that sap ascent power is of the same magnitude as a plant's metabolic budget. However, variation and uncertainty in our calculation are present due to uncertainty in the underlying data products of conductivity, a_{LAI}, canopy height, and transpiration. We estimated point by point uncertainties for biome-specific conductance values and transpiration data products. The uncertainty for both ranges up to 140% of the median value of sap ascent power with biome conductance uncertainty dominating in the tropics, while transpiration uncertainty dominates in the high latitudes (Figure S10 in Supporting Information S1). Additional sources of uncertainty in the calculation of sap ascent power, such as foliar water uptake to support transpiration, operational K_L being less than K_{max}, and uncertainty in the allometric scaling of plant resistance are typically much smaller than uncertainty in biome average K_L and in transpiration estimates (see detailed discussion in the Material and Methods). In general, even extreme estimates of their contributions are small compared to the uncertainty of plant resistance for each biome we report in the main analysis.

We found lower sap ascent power in our biome-based map of K_L (as used in the global analysis) in a comparison with a more granular community weighted approach across forests in the contiguous United States. This alternate analysis is based on *U.S. Forest Service Forest Inventory and Analysis* (FIA) data, where gridded estimates of plant K_L were derived from forest inventories and species-level data (Trugman et al., 2020). Thus, our biome-level scaling may overestimate K_L on average due to within-biome K_L variation being skewed toward a long tail of high values, combined with coarseness of global land cover maps (Figures S3 and S4 in Supporting Information S1). As a result, the median global estimates of sap ascent power presented here are likely a conservative estimate (Figures S11–S12 in Supporting Information S1). Even using the maximum and minimum estimates of K_L for each biome in forest dominated regions, we find sap ascent power to be an important source of nonmetabolic energy harvested by the plant, varying from 0.03 W/m^2 (maximum biome K_L or low resistance) to 0.88 W/m^2 (minimum biome K_L or high resistance). For a low endmember estimate of sap ascent power in forests based on maximum K_L measured in each biome, the global power needed for sap ascent is ~7.0% of photosynthetic power, while for the high-end estimate of sap ascent power (e.g., minimum biome K_L values), sap ascent power far exceeds photosynthesis (~200% p_{SA}/p_{GPP}; Figure 2).

6. High Sap Ascent Power Is Related to Climate and Physiology

Climate is an important regulator of global patterns of sap ascent power. For example, transpiration is driven by the water potential gradient along the soil-plant-atmosphere continuum, and high transpiration is possible where there is high insolation and a sufficient water supply. Tropical wet forests result in large sap ascent power values because power scales with transpiration squared (See Materials and Methods, Equation 3; Figure 3). However, physiology is also an important mediator of sap ascent power. In the tropical evergreen broadleaf forests, high K_L (per unit leaf area) and high leaf area moderate plant resistance in the tropics, as lower plant resistance allows for lower tropical sap ascent power even given the large flows of water due to the high transpiration rates (Figure 4, Equations 3, 5, and 8).

In temperate rainforests, such as the Pacific Northwest of the United States, the climate—high seasonality, lower insolation, and cooler temperatures—limits transpiration. However, physiology—particularly the lower K_L of conifers that dominate the forest in contrast to their tropical counterparts dominated by angiosperm species—still leads to high sap ascent power because of high resistance (see Materials and Methods, Equations 4–6, Figure 3). Indeed, the sap ascent power patterns are only partially related to climate (Figure 4). Even though the magnitude of the transpiration flux (which is determined both by evaporative demand and the physiology of plant water-use) drives much of the global sap ascent power, many direct climatic factors do not correlate with sap ascent power. For example, in our analysis, sap ascent power is largely independent of aridity (e.g., site water balance or precipitation divided by potential evapotranspiration), even though aridity strongly regulates global vegetation structure, physiology, and function (Choat et al., 2012; Jung et al., 2017; Quetin & Swann, 2017).

From a physiological perspective, evolutionary differences in hydraulic efficiency govern spatial patterns in sap ascent power. Angiosperm species, particularly trees such as the evergreen broadleaf trees found in high sap ascent areas of the moist tropics, have both low resistance (high K_L) values associated with their wider xylem "pipes" or vessels. In contrast, gymnosperm species have, on average, higher resistance (lower K_L) values associated with their narrower and shorter "pipes" or tracheids (Figure S2 in Supporting Information S1). These evolutionary differences in stem resistance between angiosperms and gymnosperms impact the amount of power needed during sap ascent, resulting in a similar amount of sap ascent power in relatively higher transpiration deciduous broadleaf forests and relatively lower transpiration but higher plant resistance evergreen needleleaf forests across the globe (Figure 4a). Finally, grassy plant functional types generally have low values of sap ascent power due to low whole plant hydraulic resistance and minimal influence from canopy height (see Materials and Methods). These contrasting biomes emphasize the joint regulation of physiology and climate on sap ascent power.

7. Sap Ascent Power Is a Critical Source of Energy for Forests

For forest dominated regions, the globally averaged annual energy to power sap ascent is about 14.2% of the energy in photosynthetic. Across space in forest dominated regions, this ratio of the sap ascent power to the photosynthesis power has an interquartile range of 5.9%–9.7% (using the median conductivity values for each biome) and reaches as high as 18% (99th percentile across space) in some regions (Figures 2 and 5). The energy harvested passively by the plant to power sap ascent provides a significant benefit to plant function by circulating water and hormones and drawing nutrients from the soil (Cramer et al., 2009). Critically, sap ascent power is separate from the plant's metabolism, as—beyond maintaining the hydraulic structures—the energy for sap ascent power does not have to be drawn from metabolic sources collected through photosynthesis. Rather, sap ascent power can be thought of as an additional physiological harnessing of environmental energy gradients. Though not an exact comparison, consider that humans use about 7% of their basal metabolic rate to power the heart which provides similar circulatory function (Joint & World Health Organization, 1985). In contrast, vascular plants passively harvest this energy for circulation and turn the loss of water through transpiration into a circulatory benefit that indirectly fuels life on Earth.

Globally sap ascent power generally scales positively with GPP. This is not unexpected, as sap ascent power is closely related to transpiration, which occurs in the process of photosynthesis (Equation 3). In addition, factors related to large levels of GPP—that is, tall trees and large canopies—are also closely related to the whole plant resistance (Equations 5–6). However, the slope and details of this scaling are novel. A linear fit between the mean sap ascent power and GPP power having a slope value of 0.086 (unitless; for GLEAM transpiration, slope = 0.113, for GLDAS transpiration slope = 0.059) and explaining 79% of the variance (for GLEAM 75%, and GLDAS 73%; Figure 6). There is still considerable variation in the magnitude of sap ascent power outside this general trend, highlighting the diversity in the ratio of sap ascent power to GPP across the globe (Figure 5). While the tropics have a large sap ascent power, driven predominantly by high transpiration, the large GPP of tropical wet forests decreases the relative fraction of sap ascent power (energy gained beyond the plant metabolism to power plant function) to photosynthetic power (8.3% average for the region; Figure 5). In contrast, the moderate GPP in the Pacific Northwest and the relatively high sap ascent power there, results in some of the largest power ratios globally (14.8% average for the region; Figures 5 and 6).

The increase of sap ascent power with photosynthetic power is apparent regardless of transpiration product, with important differences, particularly at high levels of photosynthesis (Figure 6). Although sap ascent power generally increases with increasing GPP, it only increases weakly for photosynthetic power less than 0.4 W/m^2 (Figure 6). When calculating sap ascent power with the GLDAS transpiration data set this trend is robust. However, the GLEAM transpiration data set shows a different relationship with a relatively sharp increase in sap ascent power after 0.4 W/m^2 of photosynthetic power. The difference in the relationship between photosynthetic power and sap ascent power, depending on the transpiration data set, highlights the potential for improving our knowledge of spatial patterns with improvements in measuring and partitioning transpiration.

For sap ascent power using GLEAM transpiration, for low values of GPP, a stable amount of sap ascent power is maintained while GPP increases. This could be due to either an increase in water-use efficiency (more GPP per transpiration) or an increase in plant conductance (transpiration increases with GPP but faces less plant resistance). For higher photosynthetic power values, sap ascent power increases in proportion to GPP. Broadly speaking, 0.4 W/m^2 of photosynthetic power appears to represent a breakpoint between ecosystems in which sap ascent power is dominated by physical factors (transpiration fluxes drive sap ascent power where sap ascent power and GPP scale positively) versus physiological factors (K_L dominates changes in sap ascent power in colder, low productivity regions).

8. Conclusion

In our analysis, we find that sap ascent power is of the same order of magnitude as the power used to fix carbon during through photosynthesis. Sap ascent power provides a significant additional energetic benefit to function in woody plants in comparison to the energy gathered through photosynthesis. Summed across forest dominated regions sap ascent power is 14.2% of the power collected through photosynthesis, with a range of 11.3%–23.1% (median, 25th–75th biome resistance) and varies across the globe from 1.5% to17.7% (1st–99th percentile) with a median value 7.8%. We note that this estimate is conservative based on a number of assumptions in the calculations. Sap ascent power is governed by the transpiration, leaf area, height, and hydraulic conductivity of an ecosystem, though none alone explain its variation across space. As expected, due to the strong covariance between photosynthesis, transpiration, and leaf area, our analysis suggests that sap ascent power is strongly related to GPP across ecosystems. However, there remains a strong variation around the general trend and significant uncertainty due to transpiration. Depending on transpiration estimates, sap ascent power and photosynthetic power are much less correlated in less productive systems because transpiration is low and physiological factors (vegetation vascular resistance to flow or the inverse of K_L) drive variations in sap ascent power, decoupling the two power values. Collectively, this study highlights how plants have evolved to passively harness pumping energy to lift water to their canopies and fuel life on Earth at a level which is comparable to modern feats of energy engineering.

Conflict of Interest

The authors declare no conflicts of interest relevant to this study.

Data Availability Statement

The conductivity data that support the findings of this study are available from Xylem Functional Trait database, https://www.try-db.org/TryWeb/Home.php. The Gross Primary Productivity data that support the findings of this study are available from https://osf.io/e9txp/files/. The North American conductivity data that support the findings of this study are available from figshare, https://figshare.com/articles/dataset/Dataset_Trait_velocities_reveal_that_mortality_has_driven_widespread_coordinated_shifts_in_forest_hydraulic_trait_composition/11962710/1. The transpiration data that support the findings of this study are available from the GLEAM database, https://www.gleam.eu/ and the GLDAS database https://hydro1.gesdisc.eosdis.nasa.gov/data/GLDAS/. The leaf area index data that support the findings of this study are available from https://sites.bu.edu/cliveg/datacodes/. The height data that support the findings of this study are available from NASA JPL at https://landscape.jpl.nasa.gov/cgi-bin/data-search.pl. The precipitation and vapor pressure deficit data that support the findings of this study area available from NCAR CRUNCEP database https://rda.ucar.edu/datasets/ds314.3/. The Potential

Evapotranspiration data that support the findings of this study are available from originator, Qiang Fu. The sap ascent power and global conductivity data generated that support the findings of this study are available at figshare along with plotting and analysis code, http://doi.org/10.6084/m9.figshare.15153117.

Acknowledgments
This work was supported by National Science Foundation Grant 2003205 and 2216855 and the United States Department of Agriculture, National Institute of Food and Agriculture, Agricultural and Food Research Initiative Competitive Programme Grant No. 2018-67012-31496. ATT acknowledges funding from the University of California Laboratory Fees Research Program Award No. LFR-20-652467. LDLA acknowledges funding from the National Science Foundation Grant 1711243. AGK acknowledges funding from the National Science Foundation DEB 1942133. The authors acknowledge User Experience and Service Designer Abigail Steinem, MDes, for design consultation on qualitative figures.

References

Ambrose, A. R. (2016). Hydraulic constraints modify optimal photosynthetic profiles in giant sequoia trees (Vol. *18*).

Anderegg, W. R. L., Konings, A. G., Trugman, A. T., Yu, K., Bowling, D. R., Gabbitas, R., et al. (2018). Hydraulic diversity of forests regulates ecosystem resilience during drought. *Nature*, *561*(7724), 538–541. https://doi.org/10.1038/s41586-018-0539-7

Anderegg, W. R. L., Trugman, A. T., Bowling, D. R., Salvucci, G., & Tuttle, S. E. (2019). Plant functional traits and climate influence drought intensification and land-atmosphere feedbacks. *Proceedings of the National Academy of Sciences*, *116*(28), 14071–14076. https://doi.org/10.1073/pnas.1904747116

Anderegg, W. R. L., Wolf, A., Arango-Velez, A., Choat, B., Chmura, D. J., Jansen, S., et al. (2018). Woody plants optimize stomatal behavior relative to hydraulic risk. *Ecology Letters*, *21*(7), 968–977. https://doi.org/10.1111/ele.12962

Badgley, G., Anderegg, L. D. L., Berry, J. A., & Field, C. B. (2019). Terrestrial gross primary production: Using NIR_V to scale from site to globe. *Global Change Biology*, *25*(11), 3731–3740. https://doi.org/10.1111/gcb.14729

Beer, C., Reichstein, M., Tomelleri, E., Ciais, P., Jung, M., Carvalhais, N., et al. (2010). Terrestrial gross carbon dioxide uptake: Global distribution and covariation with climate. *Science*, *329*(5993), 834–838. https://doi.org/10.1126/science.1184984

Berry, J. A., Beerling, D. J., & Franks, P. J. (2010). Stomata: Key players in the earth system, past and present. *Current Opinion in Plant Biology*, *13*(3), 232–239. https://doi.org/10.1016/j.pbi.2010.04.013

Bonan, G. B. (2008). Forests and climate change: Forcings, feedbacks, and the climate benefits of forests. *Science*, *320*(5882), 1444–1449. https://doi.org/10.1126/science.1155121

Brodribb, T. J. (2009). Xylem hydraulic physiology: The functional backbone of terrestrial plant productivity. *Plant Science*, *177*(4), 245–251. https://doi.org/10.1016/j.plantsci.2009.06.001

Brodribb, T. J., Powers, J., Cochard, H., & Choat, B. (2020). Hanging by a thread? Forests and drought. *Science*, *368*(6488), 261–266. https://doi.org/10.1126/science.aat7631

Brum, M., Vadeboncoeur, M. A., Ivanov, V., Asbjornsen, H., Saleska, S., Alves, L. F., et al. (2019). Hydrological niche segregation defines forest structure and drought tolerance strategies in a seasonal Amazon forest. *Journal of Ecology*, *107*(1), 318–333. https://doi.org/10.1111/1365-2745.13022

Bubb, P., May, I. A., Miles, L., & Sayer, J. (2004). Cloud forest agenda.

Burgess, S. S. O., & Dawson, T. E. (2004). The contribution of fog to the water relations of *Sequoia sempervirens* (D. Don): Foliar uptake and prevention of dehydration. *Plant, Cell, and Environment*, *27*(8), 1023–1034. https://doi.org/10.1111/j.1365-3040.2004.01207.x

Choat, B., Brodribb, T. J., Brodersen, C. R., Duursma, R. A., López, R., & Medlyn, B. E. (2018). Triggers of tree mortality under drought. *Nature*, *558*(7711), 531–539. https://doi.org/10.1038/s41586-018-0240-x

Choat, B., Jansen, S., Brodribb, T. J., Cochard, H., Delzon, S., Bhaskar, R., et al. (2012). Global convergence in the vulnerability of forests to drought. *Nature*, *491*(7426), 752–755. https://doi.org/10.1038/nature11688

Cramer, M. D., Hawkins, H.-J., & Verboom, G. A. (2009). The importance of nutritional regulation of plant water flux. *Oecologia*, *161*(1), 15–24. https://doi.org/10.1007/s00442-009-1364-3

Delzon, S., & Cochard, H. (2014). Recent advances in tree hydraulics highlight the ecological significance of the hydraulic safety margin. *New Phytologist*, *203*(2), 355–358. https://doi.org/10.1111/nph.12798

Dixon, H. H., & Joly, J. (1895). XII. On the ascent of sap. *Philosophical Transactions of the Royal Society of London B*, *186*, 563–576. https://doi.org/10.1098/rstb.1895.0012

Feng, S., & Fu, Q. (2013). Expansion of global drylands under a warming climate. *Atmospheric Chemistry and Physics*, *13*(10), 10081–10094. https://doi.org/10.5194/acp-13-10081-2013

Gleason, S. M., Westoby, M., Jansen, S., Choat, B., Hacke, U. G., Pratt, R. B., et al. (2016). Weak tradeoff between xylem safety and xylem-specific hydraulic efficiency across the world's woody plant species. *New Phytologist*, *209*(1), 123–136. https://doi.org/10.1111/nph.13646

Granier, A. (1987). Evaluation of transpiration in a Douglas-fir stand by means of sap flow measurements. *Tree Physiology*, *3*(4), 309–320. https://doi.org/10.1093/treephys/3.4.309

Hiroko, B., Rodell, M., & Huang, J. (2016). GLDAS Noah Land Surface Model L4 monthly 0.25° × 0.25° V2.1.

Holloway-Phillips, M.-M., & Brodribb, T. J. (2011). Minimum hydraulic safety leads to maximum water-use efficiency in a forage grass: Minimum hydraulic safety, maximum water-use efficiency. *Plant, Cell, and Environment*, *34*(2), 302–313. https://doi.org/10.1111/j.1365-3040.2010.02244.x

Joint, F. & World Health Organization. (1985). *Energy and protein requirements: Report of a joint FAO/WHO/UNU expert consultation [held in Rome from 5 to 17 October 1981*. World Health Organization.

Jung, M., Reichstein, M., Schwalm, C. R., Huntingford, C., Sitch, S., Ahlström, A., et al. (2017). Compensatory water effects link yearly global land CO_2 sink changes to temperature. *Nature*, *541*(7638), 516–520. https://doi.org/10.1038/nature20780

Khanna, J., Medvigy, D., Fueglistaler, S., & Walko, R. (2017). Regional dry-season climate changes due to three decades of Amazonian deforestation. *Nature Climate Change*, *7*(3), 200–204. https://doi.org/10.1038/nclimate3226

Kowalski, A. S. (2017). The boundary condition for vertical velocity and its interdependence with surface gas exchange. *Atmospheric Chemistry and Physics*, *17*(13), 8177–8187. https://doi.org/10.5194/acp-17-8177-2017

Lechthaler, S., Kiorapostolou, N., Pitacco, A., Anfodillo, T., & Petit, G. (2020). The total path length hydraulic resistance according to known anatomical patterns: What is the shape of the root-to-leaf tension gradient along the plant longitudinal axis? *Journal of Theoretical Biology*, *502*, 110369. https://doi.org/10.1016/j.jtbi.2020.110369

Liu, Y., Holtzman, N. M., & Konings, A. G. (2021). *Global ecosystem-scale plant hydraulic traits retrieved using model-data fusion*. Hydrology and Earthy System Sciences, *25*(5), 2399–2417. https://doi.org/10.5194/hess-25-2399-2021

Martens, B., Miralles, D. G., Lievens, H., van der Schalie, R., de Jeu, R. A. M., Fernández-Prieto, D., et al. (2017). GLEAM v3: Satellite-based land evaporation and root-zone soil moisture. *Geoscientific Model Development*, *10*(5), 1903–1925. https://doi.org/10.5194/gmd-10-1903-2017

Monteith, J. (1972). Solar radiation and productivity in tropical ecosystems. *Journal of Applied Ecology*, *9*(3), 747–766. https://doi.org/10.2307/2401901

Ocheltree, T. W., Mueller, K. M., Chesus, K., LeCain, D. R., Kray, J. A., & Blumenthal, D. M. (2020). Identification of suites of traits that explains drought resistance and phenological patterns of plants in a semi-arid grassland community. *Oecologia*, *192*(1), 55–66. https://doi.org/10.1007/s00442-019-04567-x

Ocheltree, T. W., Nippert, J. B., & Prasad, P. V. V. (2016). A safety vs. efficiency trade-off identified in the hydraulic pathway of grass leaves is decoupled from photosynthesis, stomatal conductance, and precipitation. *New Phytologist*, *210*(1), 97–107. https://doi.org/10.1111/nph.13781

Pathare, V. S., Sonawane, B. V., Koteyeva, N., & Cousins, A. B. (2020). C4 grasses adapted to low precipitation habitats show traits related to greater mesophyll conductance and lower leaf hydraulic conductance. *Plant, Cell, and Environment*, *43*(8), 1897–1910. https://doi.org/10.1111/pce.13807

Quetin, G. R., & Swann, A. L. S. (2017). Empirically derived sensitivity of vegetation to climate across global gradients of temperature and precipitation. *Journal of Climate*, *30*(15), 5835–5849. https://doi.org/10.1175/JCLI-D-16-0829.1

Reid, D. E. B., Silins, U., Mendoza, C., & Lieffers, V. J. (2005). A unified nomenclature for quantification and description of water-conducting properties of sapwood xylem based on Darcy's law. *Tree Physiology*, *25*(8), 993–1000. https://doi.org/10.1093/treephys/25.8.993

Ritchie, H. (2019). Our world in data energy production and consumption. Retrieved from https://ourworldindata.org/energy-production-consumption

Rodell, M., Houser, P. R., Jambor, U., Gottschalck, J., Mitchell, K., Meng, C.-J., et al. (2004). The global land data assimilation system. *Bulletin of the American Meteorological Society*, *85*(3), 381–394. https://doi.org/10.1175/BAMS-85-3-381

Sack, L., Cowan, P. D., Jaikumar, N., & Holbrook, N. M. (2003). The "hydrology" of leaves: Co-ordination of structure and function in temperate woody species. *Plant, Cell, and Environment*, *26*(8), 1343–1356. https://doi.org/10.1046/j.0016-8025.2003.01058.x

Sack, L., & Holbrook, N. M. (2006). Leaf hydraulics. *Annual Review of Plant Biology*, *57*(1), 361–381. https://doi.org/10.1146/annurev.arplant.56.032604.144141

Sack, L., & Scoffoni, C. (2012). Measurement of leaf hydraulic conductance and stomatal conductance and their responses to irradiance and dehydration using the evaporative flux method (EFM). *Journal of Visualized Experiments*(70), 4179. https://doi.org/10.3791/4179

Sack, L., & Tyree, M. T. (2005). Leaf hydraulics and its implications in plant structure and function. In *Vascular transport in plants* (pp. 93–114). Elsevier.

Schenk, H., Michaud, J., Mocko, K., Espino, S., Melendres, T., Roth, M., et al. (2020). Lipids in xylem sap of woody plants across the angiosperm phylogeny. *The Plant Journal*, *105*(6), 1477–1494. https://doi.org/10.1111/tpj.15125

Schlesinger, W. H., & Jasechko, S. (2014). Transpiration in the global water cycle. *Agricultural and Forest Meteorology*, *189–190*, 115–117. https://doi.org/10.1016/j.agrformet.2014.01.011

Scoffoni, C., Rawls, M., McKown, A., Cochard, H., & Sack, L. (2011). Decline of leaf hydraulic conductance with dehydration: Relationship to leaf size and venation architecture. *Plant Physiology*, *156*(2), 832–843. https://doi.org/10.1104/pp.111.173856

Simard, M., Pinto, N., Fisher, J. B., & Baccini, A. (2011). Mapping forest canopy height globally with spaceborne lidar. *Journal of Geophysical Research: Biogeosciences*, *116*(G4), G04021. https://doi.org/10.1029/2011JG001708

Sperry, J. S., & Love, D. M. (2015). What plant hydraulics can tell us about responses to climate-change droughts. *New Phytologist*, *207*(1), 14–27. https://doi.org/10.1111/nph.13354

Sperry, J. S., Venturas, M. D., Anderegg, W. R. L., Mencuccini, M., Mackay, D. S., Wang, Y., & Love, D. M. (2017). Predicting stomatal responses to the environment from the optimization of photosynthetic gain and hydraulic cost: A stomatal optimization model. *Plant, Cell, and Environment*, *40*(6), 816–830. https://doi.org/10.1111/pce.12852

Sperry, J. S., Wang, Y., Wolfe, B. T., Mackay, D. S., Anderegg, W. R. L., McDowell, N. G., & Pockman, W. T. (2016). Pragmatic hydraulic theory predicts stomatal responses to climatic water deficits. *New Phytologist*, *212*(3), 577–589. https://doi.org/10.1111/nph.14059

Stoy, P. C., El-Madany, T. S., Fisher, J. B., Gentine, P., Gerken, T., Good, S. P., et al. (2019). Reviews and syntheses: Turning the challenges of partitioning ecosystem evaporation and transpiration into opportunities. *Biogeosciences*, *16*(19), 3747–3775. https://doi.org/10.5194/bg-16-3747-2019

Sulla-Menashe, D., Gray, J. M., Abercrombie, S. P., & Friedl, M. A. (2019). Hierarchical mapping of annual global land cover 2001 to present: The MODIS Collection 6 Land Cover product. *Remote Sensing of Environment*, *222*, 183–194. https://doi.org/10.1016/j.rse.2018.12.013

Talsma, C. J., Good, S. P., Jimenez, C., Martens, B., Fisher, J. B., Miralles, D. G., et al. (2018). Partitioning of evapotranspiration in remote sensing-based models. *Agricultural and Forest Meteorology*, *260–261*, 131–143. https://doi.org/10.1016/j.agrformet.2018.05.010

Trugman, A. T., Anderegg, L. D. L., Shaw, J. D., & Anderegg, W. R. L. (2020). Trait velocities reveal that mortality has driven widespread coordinated shifts in forest hydraulic trait composition. *Proceedings of the National Academy of Sciences*, *117*(15), 8532–8538. https://doi.org/10.1073/pnas.1917521117

Venturas, M. D., Sperry, J. S., & Hacke, U. G. (2017). Plant xylem hydraulics: What we understand, current research, and future challenges: Plant xylem hydraulics. *Journal of Integrative Plant Biology*, *59*(6), 356–389. https://doi.org/10.1111/jipb.12534

Viovy, N. (2018). *CRUNCEP Version 7—Atmospheric Forcing Data for the Community Land Model*. Research Data Archive at the National Center for Atmospheric Research, Computational and Information Systems Laboratory. Retrieved from http://rda.ucar.edu/datasets/ds314.3/

Xiong, D., & Flexas, J. (2018). Leaf economics spectrum in rice: Leaf anatomical, biochemical, and physiological trait trade-offs. *Journal of Experimental Botany*. https://doi.org/10.1093/jxb/ery322

Zhu, Z., Bi, J., Pan, Y., Ganguly, S., Anav, A., Xu, L., et al. (2013). Global data sets of vegetation leaf area index (LAI) 3g and fraction of photosynthetically active radiation (FPAR) 3g derived from global inventory modeling and mapping studies (GIMMS) normalized difference vegetation index (NDVI3g) for the period 1981 to 2011. *Remote Sensing*, *5*(2), 927–948. https://doi.org/10.3390/rs5020927